ELSEVIER

Journal of Nuclear Materials 246 (1997) 43–52

journal of nuclear materials

High pressure hydriding of sponge-Zr in steam–hydrogen mixtures

Yeon Soo Kim [a,*], Wei-E Wang [a], D.R. Olander [a], S.K. Yagnik [b]

[a] *Department of Nuclear Engineering, University of California, Berkeley, CA 94720, USA*
[b] *Electric Power Research Institute, Palo Alto, CA 94303, USA*

Received 27 January 1997; accepted 24 March 1997

Abstract

Hydriding kinetics of thin sponge-Zr layers metallurgically bonded to a Zircaloy disk has been studied by thermogravimetry in the temperature range 350–400°C in 7 MPa hydrogen–steam mixtures. Some specimens were prefilmed with a thin oxide layer prior to exposure to the reactant gas; all were coated with a thin layer of gold to avoid premature reaction at edges. Two types of hydriding were observed in prefilmed specimens, viz., a slow hydrogen absorption process that precedes an accelerated (massive) hydriding. At 7 MPa total pressure, the critical ratio of H_2/H_2O above which massive hydriding occurs at 400°C is ~ 200. The critical H_2/H_2O ratio is shifted to $\sim 2.5 \times 10^3$ at 350°C. The slow hydriding process occurs only when conditions for hydriding and oxidation are approximately equally favorable. Based on maximum weight gain, the specimen is completely converted to δ-ZrH_2 by massive hydriding in ~ 5 h at a hydriding rate of $\sim 10^{-6}$ mol H/cm^2 s. Incubation times of 10–20 h prior to the onset of massive hydriding increases with prefilm oxide thickness in the range of 0–10 μm. By changing to a steam-enriched gas, massive hydriding that initially started in a steam-starved condition was arrested by re-formation of a protective oxide scale. © 1997 Elsevier Science B.V.

1. Introduction

Recent BWR fuel designs employ duplex cladding that has a relatively soft Zr inner liner to prevent pellet–cladding interaction (PCI). However, once a rod is defective, steam oxidation of the inner surface can generate enough hydrogen to cause severe secondary hydriding. This reaction may result in axial splits due to stress generated in the cladding during power maneuvering [1–3].

Hydrogen absorption in zirconium with a preexisting oxide scale has been investigated by several authors in atmospheric or subatmospheric pressure experiments. Gulbransen and Andrew [4] reported that the oxide film on zirconium strongly retards hydriding of the metal when exposed to hydrogen gas. These authors also investigated the permeability of prefilmed specimens to hydrogen at 300–400°C [5]. They observed two types of reactions. If the oxide film was permeable, general hydrogen absorption occurred with the formation of zirconium hydride. If the oxide film was impermeable, reaction occurred at the edges of the specimen at defects present in the oxide.

Marshall [6] reported hydrogen absorption through breakdown of the ZrO_2 film in pure hydrogen. The experiments used low pressure (< 0.01 MPa) H_2 gas. Thin ZrO_2 films from chemical polishing markedly delayed hydrogen absorption in pure hydrogen. He found that there was a delay before absorption began that was dependent on the hydrogen pressure and temperature. The fresh, presumably stoichiometric, ZrO_2 film was essentially impermeable to hydrogen gas. During exposure to H_2, the oxide film became progressively more substoichiometric. Eventually, the concentration of defects in the film became high enough to allow rapid hydrogen permeation. When localized film breakdown occurred, absorption of hydrogen led to hydride layer formation.

Oxide film breakdown was shown experimentally by Shannon [7], who demonstrated that the electrical resistance of the specimen was reduced dramatically when hydrogen started to move through the oxide film. Cox [8] investigated mechanisms of hydrogen absorption by zirconium alloys during oxidation. The most likely mechanisms

* Corresponding author. Tel.: +1-510 642 7158; fax: +1-510 643 9685; e-mail: yskim@nuc.berkeley.edu.usa.

PII S0022-3115(97)00066-4

are mechanical (rather than chemical) breakdown of the protective oxide because of compressive stresses due to the volume increase of the oxide relative to the metal consumed, formation of pores in the oxide, and stresses due to different oxidation rates of neighboring grains. Hydrogen absorption depends highly on surface treatment. Lunde [9] reported that sandblasted surfaces absorbed more hydrogen than pickled surfaces. Fluoride contamination resulted in local absorption of hydrogen. Aronson [10] experimented with plates and spheres both with and without oxide prefilming. He observed a delay of hydrogen absorption in prefilmed specimens; spheres had longer incubation times for hydrogen absorption than plates because of the smaller surface-to-volume ratio and perhaps because of the absence of sharp edges.

Smith [11] reported the hydrogen permeation rate to be approximately inversely proportional to the oxide layer thickness and directly proportional to the hydrogen pressure. The rate-determining step is diffusion across the film. Une [12] reported the incubation times as a function of preoxidized film thickness.

Zima [13] evaluated the experimental data on prefilmed Zircaloy (Zry) coupon specimens over the temperature range of 300–400°C and developed equations defining critical hydrogen-to-steam ratios below which the oxide film is protective against massive hydrogen absorption. Massive hydriding is favored when the supply of H_2O available to continuously repair the protective zirconium oxide film falls below a critical value. However, the equations are based on very limited data for Zry (for more details on the Zima model see Ref. [14]). Clayton [15] compared the calculated critical values based on the Zima model with available experimental test results.

Table 1 summarizes reported critical ratios at various temperatures at 0.1 MPa total pressure or less. The entries 10^5 in the 'critical ratio' column of Table 1 indicates that unpurified H_2 was sufficient in some cases to hydride the Zry specimens. The last row in the table represents tests performed in this laboratory in 0.1 MPa H_2. As is reported in Ref. [18], Zr/Zry/Zr sandwich specimens, crystal bar and Zry hydride in 0.1 MPa H_2 (commercial grade).

At 400°C, the higher critical ratio for crystal-bar Zr ($H_2/H_2O = 10^5$) than for Zry ($H_2/H_2O = 10^2$) is consistent with the observation reported in Ref. [18] that sponge-Zr is more resistant to hydriding than Zry. Table 1 also shows that the critical ratio increases as the temperature is decreased. However, the results in Table 1 do not reflect behavior of either Zr or Zry at reactor-operating pressure; critical H_2/H_2O ratios at 7 MPa total pressure are not available in the literature.

This paper reports the results of a program sponsored by the Electric Power Research Institute intended to obtain the hydriding kinetics of Zr-lined Zircaloy. The effects of total gas pressure and the difference between Zircaloy (Zry) and sponge-Zr liner on hydriding in commercial grade hydrogen at 400°C were reported in Ref. [18]. A brief summary of these results are: (i) the rate of massive hydriding in 7 MPa H_2 is two orders of magnitude greater than in H_2 at 0.1 MPa pressure; (ii) contrary to oxidation, Zircaloy-2 hydrides more readily than sponge-Zr. The present investigation covers a wider range of experimental variables than those tested in Ref. [18]. Experimental conditions were 7 MPa total gas pressure, temperatures of 350–400°C, preoxidized filming of the sponge-Zr, and hydrogen-steam ratios from 5–10^5. The critical hydrogen-to-steam ratio that divides regions of hydriding and oxidation was also explored.

Table 1
Comparison of critical hydrogen-to-steam ratios for massive hydriding at total pressure of 0.1 MPa or less

Material [a]	Temperature (°C)	Critical ratio [b]	Reference
Zircaloy-2	320	10^5	[16]
Zircaloy-2	400	10^2	[7]
Zircaloy-2	343	10^6–10^8	[17]
Zircaloy-2	300	10^5	[12]
Zircaloy-2	400	10^2	[12]
Crystal-bar Zr	400	10^5	present work

[a] Most specimens in this column were cut from cladding tubes or plates.
[b] A ratio of 10^5 indicates H_2 used directly from the cylinder; higher ratios mean that the gas underwent further drying and lower ratios mean that steam was added to the H_2.

The basic difference between the in-reactor situation and the laboratory tests is in the availability of hydrogen. The lab tests are of the 'unlimited hydrogen' supply type, in which the hydrogen content of the gas is unaffected by the hydriding reaction. To better simulate in the present experiments the phenomena inside an operating fuel rod when massive hydriding begins, specimens undergoing massive hydriding in pure H_2 were subjected to a rapid change of the gaseous environment to a steam–hydrogen mixture.

2. Experimental

The thermogravimetric apparatus (TGA) used to measure in situ weight changes due to reactions of the specimens in steam–hydrogen mixtures at 7 MPa and 350–400°C is shown in Fig. 1. The adaptation of the TGA method to high-pressure condensable gases is discussed in detail in Ref. [19].

Liner cladding specimens cannot be used because the different chemical reactivities of the sponge-Zr liner and the Zry outer tube cannot be separated by a single measure of reactivity (the weight gain). To avoid this difficulty, 9 mm disc specimens are cut from a specially-fabricated plate of 1 mm thick Zry (Zircaloy-2) on which layers of ~ 75 μm thick sponge Zr were co-extruded on both sides.

This sponge-Zr sandwich Zry plate (labeled Zr/Zry/Zr) was manufactured by Teledyne Wah-Chang. The sponge-Zr used by the manufacturer for the outer layer is commercial purity sponge-Zr with a total impurity content of about 2000 ppm with an oxygen level of about 1400 ppm. The Fe content is 210 ppm and the hydrogen content is 6 ppm. To avoid the deleterious effect of corners, the edges of the disk-shaped specimens are coated with a thin layer of pure gold by plasma deposition method. After the gold coating, the exposed surfaces are 7 mm circular areas. Prior to gold coating, all specimens are abraded with 1200-grit sandpaper and pickled in H_2O (50%) + HNO_3 (45%) + HF (5%) solution for 2 min. Some are then preoxidized in a steam–hydrogen or steam–helium mixture prior to the hydriding experiments [20].

Briefly, H_2 or He from cylinders are pressure-regulated to 7 MPa and flow at a rate of ~ 0.4 l/min first through the chamber housing the microbalance and then through the hot zone of the furnace in which the specimen is suspended by a fine platinum chain.

Commercial-grade hydrogen and helium gases are used. The most important impurities of hydrogen gas in hydriding experiments are oxygen and water vapor because they control the oxidant-to-hydrogen ratio. The impurity contents of hydrogen gas used in the experiments are 10 ppm O_2 and 5 ppm H_2O.

The desired steam content in the high-pressure-gas-flow stream is achieved by using a direct water feed into the flowing gas (H_2 or He) at the entry to the specimen chamber. Direct water feed provides easier operation and versatility of the system. In particular, it reduces the time for achieving the desired equilibrium steam content in the specimen chamber and enables changes of steam contents during an experiment.

The H_2/H_2O ratio is varied from 10^2–10^5 at 400°C. The lower limit H_2/H_2O ratio of 10^2 suppressed massive hydriding [20]. The H_2/H_2O ratio at 350°C is varied from 10^3–10^5.

The cross-section surfaces of reacted disk specimens were optomicroscopically examined to show hydride precipitates or oxide layers. For this purpose, the surfaces were swab-etched with 60% H_2O_2 + 39% HNO_3 + 1% HF solution for ~ 2 min after polishing of the cross-section surface.

The amount of hydrogen absorbed in the specimen determines whether the specimen is predominantly hydrided or oxidized in a given steam–hydrogen mixture. Since the hydriding rate is very slow at the critical steam-to-hydrogen ratio, determination of the origin of the observed weight gain is made by a post-test measurement of the hydrogen content of the reacted specimen. A specially-built hydrogen analyzer is used to determine the hydrogen content in reacted specimens. The hydrogen analyzer uses the method of hot extraction of hydrogen absorbed in samples by heating the reacted specimen to ~ 1500°C (see Ref. [21]).

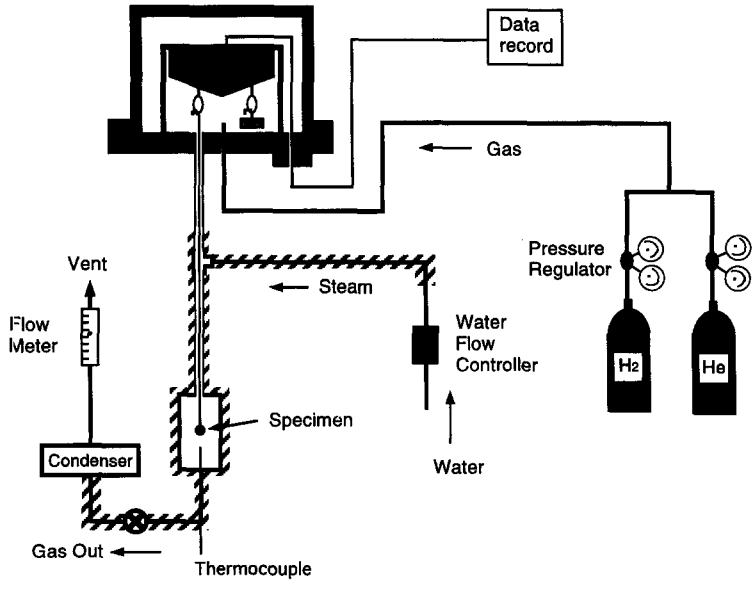

Fig. 1. Schematic diagram of high-pressure thermobalance system.

3. Results and discussion

3.1. Reaction at 400°C

Table 2 lists the results from experiments at 400°C in 7 MPa steam (< 10%)-hydrogen mixtures. Numerous runs were made at this temperature to determine the critical H_2/H_2O ratio.

3.1.1. Effect of prefilming

Hydriding of three Zr/Zry/Zr disk specimens with different prefilm oxide thicknesses in commercial-grade hydrogen ($H_2/H_2O \sim 10^5$) is shown in Fig. 2. A weight gain of ~ 11 mg corresponds to complete conversion of the specimen to δ-ZrH_2. The sharp weight losses especially evident in run OP61 are caused by chips of hydride that have flaked off the specimen. The bare specimen that had no preoxidized film (Run OP57) hydrided without an incubation period at a rate of 1.5×10^{-6} mol H/cm^2 s. As the preoxidized film thickness increased the incubation time for massive hydriding increased (Runs OP61 and OP63). The massive hydriding rate for these experiments is ~ 10^{-7} mol H/cm^2 s, which is slower than that of the bare specimen. Although the massive hydriding rates are calculated based on weight gain and reaction surfaces, this does not imply that massive hydriding is uniform over the specimen surfaces (see Fig. 6).

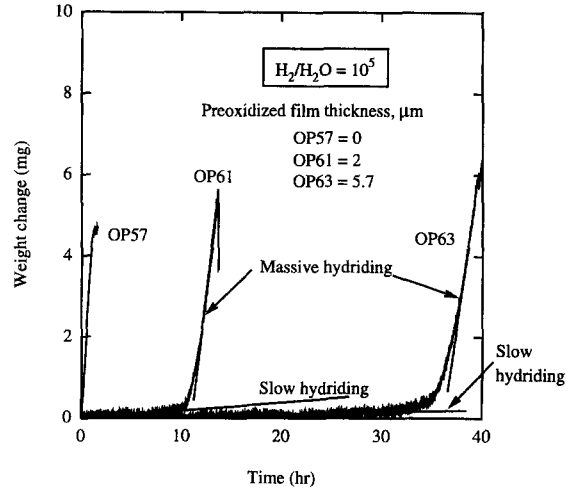

Fig. 2. Hydriding of Zr/Zry/Zr at 7 MPa and 400°C in commercial-grade hydrogen.

Table 2
Reactions of Zr/Zry/Zr at 400°C in 7 MPa steam–hydrogen mixtures

Run No.	H_2/H_2O ratio	Preoxidized film thickness (μm)	Oxidation rate [a] (mol O/cm^2 s) $\times 10^{-10}$	Slow hydriding rate (mol H/cm^2 s) $\times 10^{-8}$	Massive hydriding rate (mol H/cm^2 s) $\times 10^{-7}$	Incubation time for massive hydriding (h)	Hydrogen content (wppm)	Hydrogen pickup ratio [e]
OP57	10^5	0	[b]	0	15.2	0	–	–
OP61	10^5	2 (B)	[b]	0.8	6.6	10	–	–
OP63	10^5	5.7 (W)	[b]	3.6	5.2	35	–	–
OP99	10^3	0.9 (W)	[b]	3.6	14.45	1	–	–
OP58	2×10^2	0	[b]	0	14	0	–	–
OP60	2×10^2	0	[b]	0	12	0	–	–
OP72	2×10^2	1.1 (B)	2.3	0.6	NA	NA	840	10.64
OP70	2×10^2	2.1 (B)	0.5	0.03	[c]	NA	712	4.01
OP53	2×10^2	2.9 (B) [d]	0.5	0.01	[c]	NA	87	0.75
OP50	2×10^2	4.9 (W) [d]	[b]	4.2	4.2	9	–	–
OP85	2×10^2	7.5 (W)	[b]	0	19	0	–	–
OP66	10^2	0	2.3	[c]	[c]	NA	–	–
OP67	10^2	0	1.1	0.02	[c]	NA	349	1.30
OP68	10^2	0	2.2	0.08	[c]	NA	392	2.47
OP51	77	3 (B) [d]	2.1	[c]	[c]	NA	–	–
OP52	20	0	2.6	0.02	[c]	NA	95	0.47

[a] To determine the rate of oxidation, specimen weight gains were first corrected for hydrogen absorption when this measurement was available.
[b] Hydriding, no observable oxidation.
[c] Oxidation dominant.
[d] Preoxidized in 1 atm steam.
[e] Ratio of amount of hydrogen absorption to amount of hydrogen production by oxidation.
B: black oxide.
W: white oxide.
NA: Not applicable.

3.1.2. Slow hydriding and massive hydriding

Two modes of hydriding of Zr/Zry/Zr with prefilmed oxide scale were observed (see Table 2). OP61 and OP63 in dry hydrogen showed the initial slow rate then the second fast rate. This phenomenon was also found in OP99, OP72 and OP50 which were conducted in mixed gases of steam and hydrogen. The first hydriding process may be due to slow absorption of hydrogen through thin oxides. This process appears to be distinct from the commonly-observed 'pickup' of hydrogen released by reaction with water. As seen in the last column of Table 2, the hydrogen pickup ratios are generally greater than unity, indicating that some part of the absorbed hydrogen originates from direct absorption of gaseous H_2. The oxide eventually cracks due to the volume expansion of absorbed hydrogen precipitated under the oxide. At this time, direct absorption of hydrogen through the bare surface becomes possible. The absorption rate at this stage is much higher than the first slow hydriding rate. Typically, the slow hydriding rate is $\sim 10^{-8}$ mol H/cm^2 s and the fast (massive) hydriding rate is $\sim 10^{-6}$ mol H/cm^2 s.

If the slow weight gain preceding massive hydriding were due only to oxidation, massive hydriding would never occur because of the increasing resistance to hydrogen induced breakdown of the thickening oxide. The weight gain rate of slow hydriding, however, is of the order of the weight gain rate due to oxidation at the same temperature. However, the hydrogen content of the reacted specimen of OP72, for which the experiment was terminated before massive hydriding occurred, was 40 times larger than the normal oxidation pickup fraction (~ 0.25) (see Table 2). About 60% of the total weight gain was due to hydrogen absorption and 40% was due to oxidation. This confirms that oxidation and slow hydriding were progressing simultaneously.

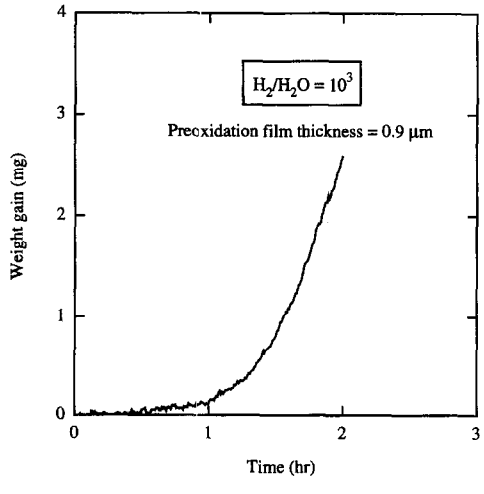

Fig. 3. Hydriding of Zr/Zry/Zr at 7 MPa and 400°C in steam–hydrogen mixture (OP99).

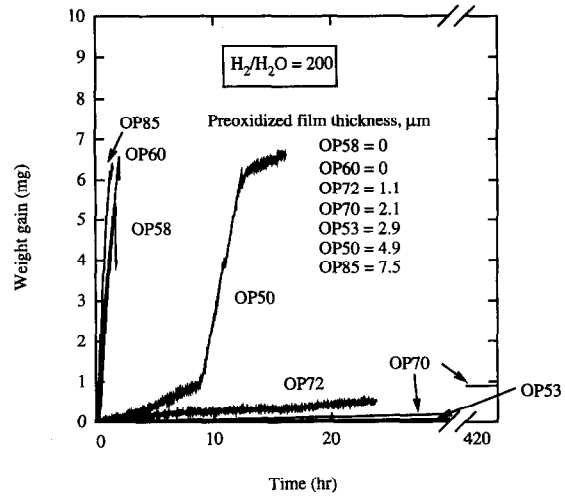

Fig. 4. Hydriding of Zr/Zry/Zr at 7 MPa and 400°C in 0.5% steam–99.5% hydrogen mixture.

One run with a hydrogen-to-steam mole ratio of 10^3 was performed (OP99). The hydriding weight gain is shown in Fig. 3. Massive hydriding initiated after an incubation period of ~ 1 h. The slow and massive hydriding rates are 3.6×10^{-8} mol H/cm^2 s and 1.4×10^{-6} mol H/cm^2 s, respectively.

3.1.3. Effect of steam concentration

The massive hydriding rate does not depend on the steam concentration in the hydrogen gas (see Table 2). The massive hydriding rate of OP57 with no prefilmed oxide for $H_2/H_2O = 10^5$ is 1.5×10^{-6} mol H/cm^2 s and that of OP58 with no prefilmed oxide for $H_2/H_2O = 2 \times 10^2$ is 1.4×10^{-6} mol H/cm^2 s. This means that hydrogen absorption, rather than oxidation, is the dominant reaction in steam–hydrogen mixtures if the H_2/H_2O ratio is above the critical value. The tests in ~ 1 mol% steam in Table 2 all exhibited oxidation behavior only, even with no prefilm oxide scale. This steam content is clearly protective to massive hydriding, although slow hydriding occurs. Run OP52, using 5 mol% steam, is also clearly oxidizing.

3.1.4. Effect of oxide prefilming at the critical H_2/H_2O ratio

The hydriding curves of Zr/Zry/Zr specimens for $H_2/H_2O = 200$ at 7 MPa and 400°C are plotted in Fig. 4. As discussed later, this H_2/H_2O ratio is close to the critical value for this temperature. The bare specimens (OP58 and OP60) started massive hydriding immediately at a rate of $1.2–1.4 \times 10^{-6}$ mol H/cm^2 s. The other preoxidized specimens, even with very thin oxide films, showed significant differences from the bare specimen. Run OP72 with a 1 μm oxide film showed an initial hydriding rate (0.9×10^{-8} mol H/cm^2 s) which was much

lower than those of the unprotected specimens. This experiment was terminated before massive hydriding occurred.

The protection capability of oxide films where the H_2/H_2O ratio is close to the critical value is shown better in Run OP70, which lasted for 421 h without hydriding (see Fig. 4). A comparison of Run OP61 shown in Fig. 2 (hydriding in H_2/H_2O 10^5) with Run OP70 (no hydriding in $H_2/H_2O = 200$), both having approximately the same preoxidized film thickness, shows that decreasing the H_2/H_2O to 200 causes the preoxidized film to stay effective in protecting the metal from hydriding.

The weight–gain rates of runs OP70 and OP53 are those of oxidation, not hydriding. Whatever the origin of the weight gains, Fig. 5 shows that prefilm oxide thicknesses between 2 and 3 μm produce the lowest weight–gain rates and, at least in the time frame of the experiments, prevent massive hydriding at $H_2/H_2O = 200$. Fig. 5 is an example of the coexistence of all three reaction regimes, namely, massive hydriding, slow hydriding, and oxidation. This is possible only at or near to the critical H_2/H_2O ratio. If the H_2/H_2O ratio is greater than the critical value, massive hydriding cannot be prevented; the prefilm oxide thickness affects only the incubation period prior to the onset of massive hydriding. If H_2/H_2O ratio is less than the critical value, oxidation with slow hydriding takes place (see the last five runs in Table 2).

Optical photomicroscopy of specimen OP72 shows a high density of hydride platelets distributed uniformly throughout the specimen cross-section (Fig. 6). In addition, the sponge-Zr layer has heavily hydrided local spots. This also supports the claim that slow hydriding was progressing. The preoxidized specimen used for this hydriding experiment was obtained from the batch oxidizing experiment with the specimen (Run OP71), for which the conditions were 350°C and 7 MPa in 5% steam.

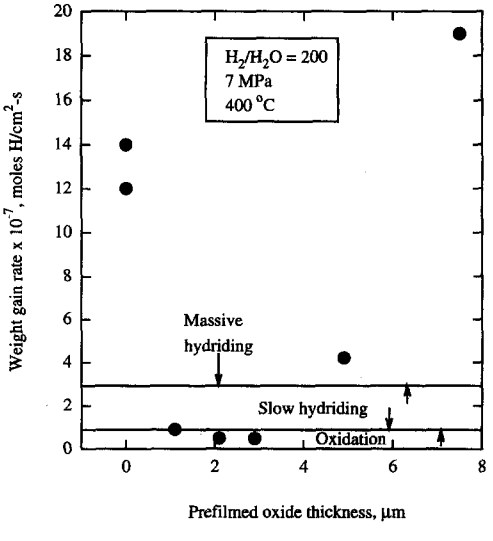

Fig. 5. Effect of prefilmed oxide thickness on the weight gain rate at the critical H_2/H_2O ratio.

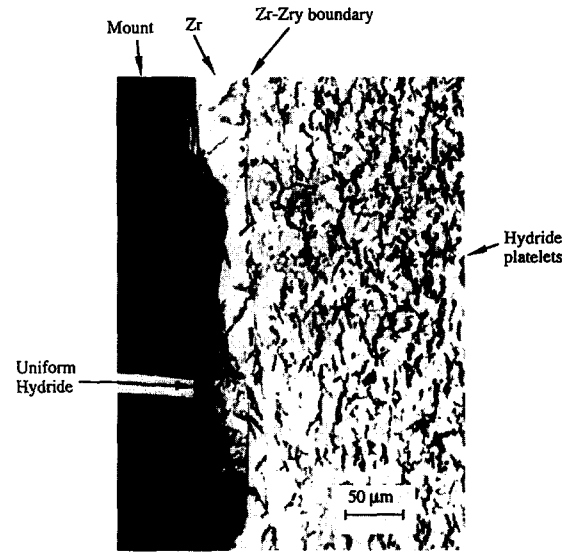

Fig. 6. Cross section view of Zr/Zry/Zr hydrided in 0.5% steam–99.5% hydrogen mixture at 7 MPa and 400°C (OP72).

The critical ratio is not a sharp boundary between massive hydriding and oxidation but rather a fuzzy separation. Whether massive hydriding occurs or not depends mainly on the material, specifically on the characteristics of the oxide on it, and, as seen in Fig. 5, on the oxide scale thickness.

3.1.5. Effect of prefilm morphology

Of the experiments conducted with $H_2/H_2O = 200$ at 400°C, four (OP85, OP50, OP58 and OP60) clearly exhibited massive hydriding. Two others (OP70 and OP53) experienced only oxidation. OP50 is anomalous. It clearly hydrided, exhibiting both slow and massive hydriding rates in the expected ranges for these two processes. However, the prefilmed oxide scale thickness of ~5 μm should have prevented hydriding entirely, based on the experience of runs OP53, OP70, and OP72, or at least should have shown long incubation period. OP61 which used commercial-grade hydrogen and thinner oxide exhibited a longer incubation time than OP50. This apparent inconsistency is explained by the characteristics of the preoxidized film. It is observed that oxide with white patches (OP50, OP85) is not protective. When the sponge-Zr layer is exposed to the reactants, it tends to produce white nodular oxide in the long run. As the oxide grows, it is increasingly likely to convert to white oxide [21]. This explains why thicker oxide is less protective. Since the onset of white pustular oxide depends on temperature, reacting gas, and composition of sponge-Zr, it is impossible to predict whether a given oxide is protective. Specimen OP85, with a thick

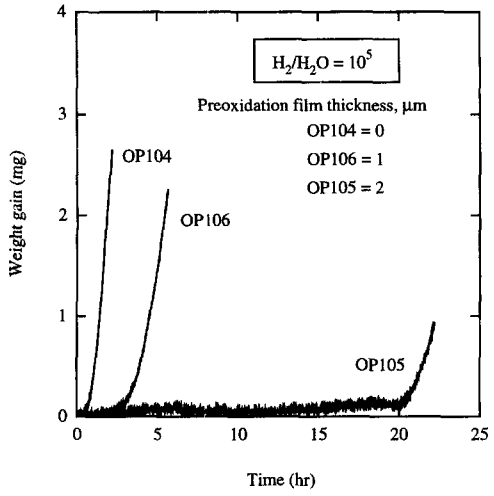

Fig. 7. Hydriding of Zr/Zry/Zr at 7 MPa and 350°C in commercial-grade hydrogen.

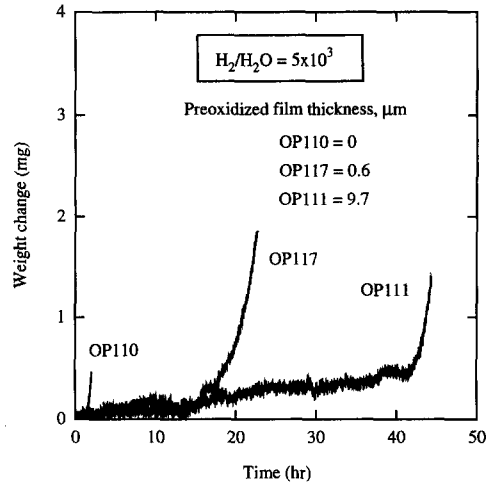

Fig. 8. Hydriding of Zr/Zry/Zr at 7 MPa and 350°C in 0.02% steam–99.98% hydrogen mixture.

oxide prefilm (~ 7.5 μm), hydrided rapidly almost from the start of the experiment at a rate higher than those of the bare specimens OP58 and OP60.

3.2. Reaction at 350°C

A smaller number of runs were made at 350°C because the search for the critical value of H_2/H_2O had become more efficient. The runs performed for finding the critical steam-to-hydrogen ratio at 350°C are summarized in Table 3.

3.2.1. Effect of prefilm thickness

Fig. 7 shows hydriding weight gain histories of three runs in 7 MPa commercial-grade hydrogen ($H_2/H_2O = 10^5$) at 350°C. The specimen without preoxidized film (OP104) hydrided without incubation period. The hydriding rate of OP104 is 4.5×10^{-7} mol H/cm^2 s while the hydriding rate of its counterpart (OP57) at 400°C is 1.5×10^{-6} mol H/cm^2 s. The massive hydriding rate is slower for thicker preoxidized specimen (see Table 3). The specimens with preoxidized films showed incubation periods before massive hydriding occurred. Comparing with Fig. 7 with its counterpart at 400°C, Fig. 2, it appears that the incubation periods are halved at the higher temperature.

Fig. 8 shows hydriding weight gain histories of specimens for $H_2/H_2O = 5000$ at 350°C. The bare-metal specimen (OP110) hydrided massively immediately at a rate of 2.4×10^{-7} mol H/cm^2 s. As the preoxidized film thickness increases, the incubation time also increases.

Table 3
Reactions of Zr/Zry/Zr at 350°C in 7 MPa steam–hydrogen mixtures

Run No.	H_2/H_2O ratio	Preoxidized film thickness (μm)	Oxidation rate (mol O/cm^2 s) $\times 10^{-10}$	Slow hydriding rate (mol H/cm^2 s) $\times 10^{-8}$	Massive hydriding rate (mol H/cm^2 s) $\times 10^{-7}$	Incubation time for massive hydriding (h)	Hydrogen content (wppm)	Hydrogen pickup ratio [a]
OP104	10^5	0	0	0	4.5	0	–	–
OP106	10^5	1 (B)	0	1.0	2.6	2.5	–	–
OP105	10^5	2 (B)	0	0.2	1.2	20	–	–
OP110	5×10^3	0	0	0	2.4	0.5	–	–
OP117	5×10^3	0.6 (B)	0	0.5	1.8	15	–	–
OP111	5×10^3	9.7 (W)	0	0.4	1.4	42	–	–
OP109	10^3	0	0.5	0	0	NA	–	–
OP108	2×10^2	0	1.2	0	0	NA	184	13.67
OP103	33	0	1.0	0	0	NA	132	1.81

[a] Ratio of amount of hydrogen absorption to amount of hydrogen production by oxidation.
NA: Not applicable.
B: black oxide.
W: white oxide.

3.2.2. Effect of H_2/H_2O ratio

The effect of steam concentration in hydrogen on massive hydriding at 7 MPa is shown in Fig. 9. OP106 with a prefilmed oxide hydrided for $H_2/H_2O = 10^5$ and OP117 with a thinner oxide than OP106 also hydrided for $H_2/H_2O = 5 \times 10^3$. Massive hydriding did not occur for $H_2/H_2O = 10^3$, or for any H_2/H_2O ratio below this value. Therefore, the critical H_2/H_2O value lies between 5×10^3 and 1×10^3 at 350°C. No runs were performed at the critical H_2/H_2O ratio at 350°C. As at 400°C, the massive hydriding rate does not depend on the steam concentration in the hydrogen gas at 350°C (see Table 3).

3.2.3. Comparison with hydriding at 400°C

A general comparison of hydriding reactions between 350 and 400°C is given in Table 4. Both the 'slow' and massive hydriding rates are faster at 400°C by a factor of ~ 3 than at 350°C. The critical H_2/H_2O ratio separating regions of oxidation and hydriding is an order of magnitude larger at the lower temperature than at the higher one. At both temperatures, the rates of hydriding and oxidation are independent of H_2/H_2O ratio as long as this ratio was well in one of the reaction regimes.

3.3. In-reactor hydriding mechanism

Massive hydriding starts when the H_2/H_2O ratio rises above a critical value. Since this form of hydriding is fast, once initiated, it inexorably leads to total consumption of the specimen as long as the gas composition remains constant. However, failed cladding from in-reactor operation characteristically shows partial localized hydriding in the form of sunbursts [22,23]. This arrested hydriding process suggests the following in-reactor mechanism. If the steam-starved condition is met in the gap in the fuel rod, the weakest spot in the vicinity develops a local hydriding by massive hydrogen absorption. Hydrogen removal from the gas causes the local steam concentration to increase and the total pressure to drop. The increase in local steam concentration decreases the H_2/H_2O ratio below the critical value, resulting in cessation of massive hydriding. In response to the decrease in total pressure, steam is resupplied through the primary defect hole to re-establish pressure equilibrium. The gas mixture arriving at the locally hydrided spot is steam-enriched, and thus promotes reformation of the protective oxide at the hydrided spot. Another localized hydriding results when the gas dries out and becomes richer in hydrogen again by continued oxidation. Repetition of this process may produce many sunburst type hydrides in regions of the rod far from the primary defect.

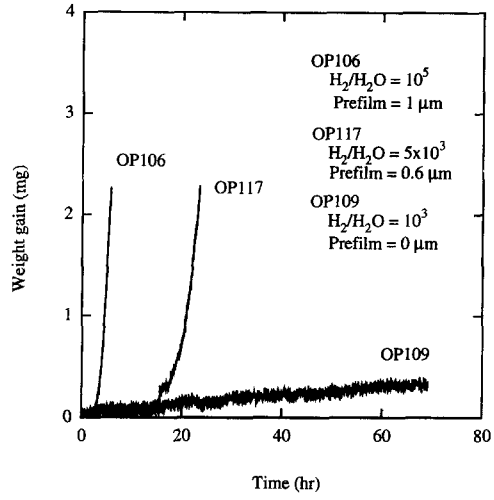

Fig. 9. Effect of steam content on massive hydriding of Zr/Zry/Zr at 7 MPa and 350°C.

The experiments described in Sections 3.1 and 3.2 were conducted in gases with fixed H_2/H_2O ratios. As discussed above, this condition does not reflect the limited quantity of hydrogen available for reaction in the fuel-cladding gap of a defective fuel rod. To simulate the latter, experiments were conducted with H_2/H_2O ratio initially above the critical value. Past way through massive hydriding, the steam content was increased to determine whether massive hydriding could be arrested.

Fig. 10 shows the weight gain history at 7 MPa and 400°C. Massive hydriding starts from time zero in commercial-grade hydrogen (region A). After 1 h, the steam concentration of the gas was increased to 2%. The weight gain rate decreased dramatically (region B). However, the weight gain curve still showed a higher weight gain rate than a normal oxidation rate although the H_2/H_2O ratio was below the critical value. The reaction in this region can be characterized as follows.

Table 4
General comparison between 7 MPa hydriding data from 350 and 400°C

Item	350°C	400°C
Slow hydriding rate ($\times 10^{-8}$ mol H/cm^2 · s)	0.4–1.0	0.8–4.2
Massive hydriding rate ($\times 10^{-7}$ mol H/cm^2 · s)	1.2–4.5	5.2–19
Critical H_2/H_2O ratio	2500	200
Effect of steam concentration on the hydriding rate above the critical H_2/H_2O ratio	none	none
Effect of steam concentration on the oxidation rate below the critical H_2/H_2O ratio	none	none

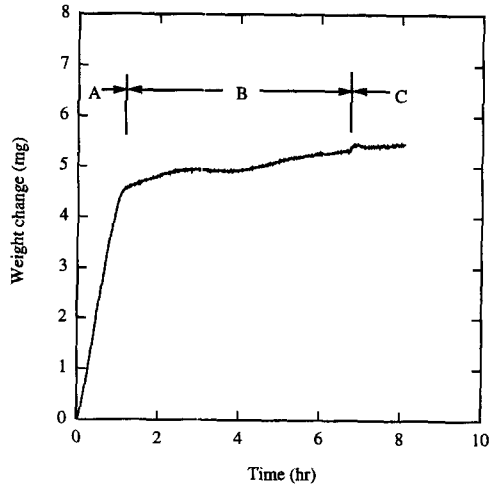

A: massive hydriding ($H_2/H_2O = 10^5$)
B: retardation of massive hydriding ($H_2/H_2O = 50$)
C: termination of massive hydriding ($H_2/H_2O = 25$)

Fig. 10. Termination of massive hydriding of Zr/Zry/Zr at 7 MPa and 400°C in steam enriched hydrogen gas (OP57).

(i) The early stage of reaction of region B must be deceleration of massive hydriding in a gas of gradually increasing steam content. As was discussed in Section 3.1, the critical H_2/H_2O value is not a sharp boundary between hydriding and oxidation, so hydrogen absorption was still the dominant reaction for this stage although H_2/H_2O ratio was below the critical value. Oxidation started reforming a protective oxide simultaneously.

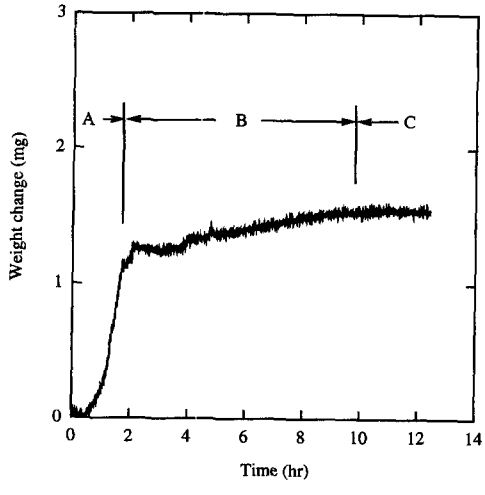

A: massive hydriding ($H_2/H_2O = 10^5$)
B: retardation of massive hydriding ($H_2/H_2O = 10^3$)
C: termination of massive hydriding ($H_2/H_2O = 2 \times 10^2$)

Fig. 11. Termination of massive hydriding of Zr/Zry/Zr at 7 MPa and 350°C in steam enriched hydrogen gas (OP112).

(ii) As a protective oxide film was reformed, the hydrogen absorption rate decreased, resulting in a gradual flattening of the weight gain curve toward the end of the region B.

Five hours later the steam content was increased to 4%. Only oxidation continued for this interval. The experiment was terminated when hydriding had been stopped. Only the much slower oxidation process, not be detectable on the time scale of the test, continued in region C.

Fig. 11 shows the weight gain history of the specimen at 7 MPa steam–hydrogen mixtures at 350°C. Again massive hydriding was first slowed and then terminated when the gas was enriched with steam. Lower steam concentrations were needed to terminate massive hydriding at 350°C than at 400°C.

These results do not constitute evidence for sunburst-type hydriding but rather show that an arrest or retardation of massive hydriding can be achieved by increasing the steam content in the hydrogen–steam mixtures.

4. Conclusions

From this series of experiments at 7 MPa pressure and 350–400°C, the following can be concluded.

(1) Commercial-grade hydrogen with no added steam ($H_2/H_2O = 10^5$) hydrides the Zr/Zry/Zr sandwich specimens no matter what thickness of prefilm oxide scale is used. If the oxide is black and protective, prefilming serves to delay massive hydriding, with the incubation period increasing with increasing oxide film thickness.

(2) Two modes of hydriding rates of Zr/Zry/Zr are observed: the first is slow, with a rate of $\sim 10^{-8}$ mol H/cm^2 s and the second is accelerated, with a rate of $\sim 10^{-6}$ mol H/cm^2 s.

(3) The massive hydriding rate does not depend on the H_2/H_2O ratio of the gas.

(4) For $H_2/H_2O = 200$ at 7 MPa and 400°C, hydriding and oxidation are in rough balance within the time frame of the experiments; with no oxide prefilm, hydriding occurs immediately; with oxide scales between 1 and 3 μm thick, hydriding appears to be suppressed in favor of continued oxidation. However, specimens with thicker oxide scales hydrided. This demonstrated a maximum in the protection capability of oxide prefilms at intermediate thickness.

(5) If the H_2/H_2O ratio is greater than the critical value, massive hydriding occurs regardless of the prefilmed oxide. If the H_2/H_2O ratio is less than the critical value, oxidation continues. However, the critical value is not sharp but occurs over a range of H_2/H_2O ratios. In this range slow hydriding and oxidation occur simultaneously. At 7 MPa, for 400°C $H_2/H_2O = 2 \times 10^2$; for 350°C $H_2/H_2O = 2.5 \times 10^3$ are the midvalues of the ranges that separate oxidation and hydriding.

(6) White nodular oxides that are observed more fre-

quently on sponge-Zr than on Zry are more vulnerable to massive hydrogen attack.

(7) Rapid hydriding of Zr/Zry/Zr initially begun in H_2/H_2O ratios above the critical value can be stopped when steam-enriched gas above the critical H_2/H_2O ratio is introduced.

References

[1] K. Lin et al., Investigation on the post-defect deterioration of nonbarrier BWR rods, Proceedings of the 1994 international topical meeting on light water reactor fuel performance, West Palm Beach, FL, 1994.
[2] J.S. Armijo, Performance of failed BWR fuel, Proceedings of the 1994 international topical meeting on light water reactor fuel performance, West Palm Beach, FL, 1994.
[3] D. Schrire et al., Secondary defect behavior in ABB BWR fuel, Proceedings of the 1994 international topical meeting on light water reactor fuel performance, West Palm Beach, FL, 1994.
[4] E.A. Gulbransen, K.F. Andrew, J. Electrochem. Soc. 101 (1954) 348.
[5] E.A. Gulbransen, K.F. Andrew, J. Electrochem. Soc. 104 (1957) 709.
[6] R.P. Marshall, J. Less-Common Met. 13 (1967) 45.
[7] D.W. Shannon, Corrosion 19 (1963) 414t.
[8] B. Cox, Mechanisms of hydrogen absorption by zirconium alloys, Atomic Energy of Canada Limited, AECL-8702, 1985.
[9] L. Lunde, J. Nucl. Mater. 44 (1972) 241.
[10] S. Aronson, Some experiments on the permeation of hydrogen through oxide films on zirconium, WAPD-BT-19, 1960.
[11] T. Smith, J. Nucl. Mater. 18 (1966) 323.
[12] K. Une, J. Less-Common Met. 57 (1978) 93.
[13] G.E. Zima, A review of the Zircaloy-2 hydriding program, HW-66537, 1960.
[14] D.R. Olander, S. Vaknin, Secondary hydriding of defected Zircaloy-clad fuel rods, Electric Power Research Institute, EPRI TR-101773, 1993.
[15] J.C. Clayton, Internal hydriding in irradiated defected Zircaloy fuel rods, Zirconium in the nuclear industry: Eighth international symposium, ASTM STP 1023, American Society for Testing and Materials, Philadelphia, 1989, p. 266.
[16] R.L. Gibby, Hydriding of PRTR fuel rod end caps, BNWL-150, 1965.
[17] R.F. Boyle, T.J. Kisiel, Hydrogen permeation of Zircaloy-2 corrosion films, WAPD-BT-10, 1958.
[18] Y.S. Kim et al., J. Nucl. Mater. 240 (1996) 27.
[19] Y.S. Kim et al., Application of thermogravimetry in high pressure, high temperature condensable gas environments, High Temperatures – High Pressures, 27/28 (1995/1996) 555.
[20] Y.S. Kim et al., J. Nucl. Mater. 245 (1997) 152.
[21] D.R. Olander et al., Investigation of the roles of corrosion and hydriding of barrier cladding and fuel pellet oxidation in BWR fuel degradation, Proceedings of the 1997 international topical meeting on LWR fuel performance, Portland, Oregon, March 1997, p. 149.
[22] D.H. Locke, Nucl. Eng. Design 21 (1972) 318.
[23] F. Garzarolli, R. von Jan, H. Stehle, At. Energy Rev. 1 (1979) 31.